Preprints of the 21st IFAC World Congress (Virtual)
Berlin, Germany, July 12-17, 2020

Path Tracking Control for Urban Autonomous Driving

.

Christian Klauer * **Manuel Schwabe** * **Hamid Mobalegh** *

* *TomTom, Berlin, Germany (e-mail: christian.klauer@tomtom.com).*

Abstract: A path tracking controller for autonomous vehicles in urban environments is presented. Based on system inversion, the steering angle causing the vehicle to follow the path in absence of disturbances is calculated. Then, the lateral distance and the orientation error w.r.t. the path are compensated by a state feedback controller. Further, a decoupling of the velocity is considered in the system-inversion and the feedback controller. Therefore, ideally, the velocity does not influence path tracking and, hence, the requirements on velocity control are relaxed. To reduce the effort for parameter identification, the controller is intentionally based on a kinematic vehicle model requiring less parameters compared to an elaborated dynamic model. It is assumed that the effects of unconsidered system components, e.g., tire slip, are then compensated by the state-feedback controller. The approach is validated on a closed proving-ground in a simulated urban scenario. Herein, for driving velocities up to 14 m/s and curve radii of down to 10 m, an RMS tracking error for the lateral distance to the path of 7.2 *cm* was achieved. The control system will be used in TomTom's autonomous car 'Trillian' that serves as a validation and research platform to evaluate high definition maps of road networks.

Keywords: Vehicle dynamic systems, Nonlinear and optimal automotive control

1. INTRODUCTION

In the field of autonomous driving vehicles, path tracking control is a common approach to realize automatic steering of the vehicle. Therefore, a reference trajectory is computed by a motion planning algorithm that incorporates obstacle information derived from environmental perception information (e.g., obtained by lidars, radars, ...) to avoid obstacle collisions. Further, road geometry information and possible driving-paths, typically stored in a map, serve the motion planner. Using a feedback of the vehicle position, heading, and velocity, a steering and velocity control system tracks the trajectory [Paden et al. (2016)].

Among the investigated approaches are linear control systems (e.g., PID, H_∞) and nonlinear approaches, e.g., based on differential flatness, backstepping, ...

Despite coupled longitudinal (velocity) and lateral (steering) dynamics, in some approaches, the control of steering and velocity are treated separately [Khodayari et al. (2010)]. However, the tracking performance in curves might be limited. A linear steering controller is described in [Marino et al. (2011)]. The control system consists of an underlying heading controller (PD-control) and a lateral position PID-controller in an outer-loop.

To improve the lateral tracking performance, control systems that combine lateral and longitudinal control using MIMO-control were considered. An example is given by [Menhour et al. (2014)] who propose a flatness-based controller to improve the performance in curves. The controller is based on a model describing three DoF (position on a surface, and heading) of the car motion-dynamics. To achieve the improved tracking performance, however, the system model including, e.g., tire parameters must be known. A similar approach is given in [Xia et al. (2016)].

A simple and effective tracking controller is described in [Thrun et al. (2006)]. Herein, the front wheel of a kinematic bicycle model is controlled using an inversion of the model. A feedback controller then compensates the lateral displacement from the path. To control driving using a vision-based path recognition system, a controller based on backstepping and sliding mode is proposed by [Guo et al. (2016)]. The aim is to track a path and to compensate for lateral errors measured ahead of the vehicle determined by the vision system.

Recently it became more common to apply model predictive control (MPC) in its linear and nonlinear variants. To reduce the computational effort, [Falcone et al. (2007)] suggested a linear MPC with online-linearized model and compared it to nonlinear MPC. In nonlinear MPC, though the computational constraints became – due to the increased computational capabilities – recently more relaxed, still difficulties in proving the stability of the closed-loop systems exist [Paden et al. (2016)]. In linear MPC, the nonlinear model can be linearized for the current operational point. However, along the prediction horizon, the prediction accuracy typically decreases reducing the controller performance compared to nonlinear MPC.

A recently published approach is to realize path tracking using the Newton-Raphson flow with the advantage of less computational effort compared to MPC [Shivam et al. (2019)]. The research is still in an early stage, however.

To improve tracking performance, system inversion and MPC approaches (as listed above) often rely on elaborated dynamic models. Herein, often, the knowledge of mechanical masses and moments of inertia is assumed. Further, models to describe the tire-slip are often used to describe the contact forces to the ground.

To reduce the effort spent for gaining system knowledge, e.g., by system identification, this contribution, in contrast, intentionally focuses on a simpler kinematic model that relies on less parameters. The model is used to calculate the steering angle to realize path tracking in absence of disturbances or model uncertainties. Deviations in terms of heading and lateral distance to the path are then compensated by a feedback controller that operates on a virtual steering control input introduced by the inversion.

In longitudinal control, combustion engines are known for complex nonlinear dynamics. Hence, tracking the velocity with a precision high enough not degrading the path tracking performance might be challenging [Attia et al. (2014)]. Hence, in the presented work, the path tracking is designed to be independent of the vehicle velocity. Thus, the performance requirements on the velocity tracking are relaxed. Then, a 2DoF PI-controller is assumed to be sufficient, which reduces the required knowledge of vehicle parameters even further.

Lastly, the controller initialization, i.e., the handover from a manual driver in case of lateral and heading errors w.r.t. to the path is considered. Therefore, a path-approaching controller is presented that limits motion-jerk even if the vehicle is not aligned to the path on handover.

Our approach is similar to [Thrun et al. (2006)], however, a vehicle orientation stabilization and measures for controller initialization are added. Further, the non-linear dynamics of the steering actuator is considered.

2. OVERVIEW

The set-up to control the car (Volvo XC-90, Volvo Car Corporation, Göteborg, Sweden) is shown in Fig. 1. The vehicle provides a drive-by-wire interface which is accessible by a CAN-interface.

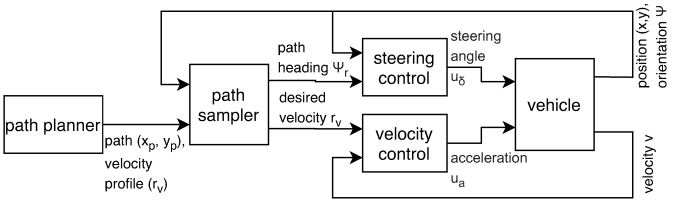

Fig. 1. System overview.

An upper-level path- and velocity planner (not considered in this contribution) generates reference trajectories for driving. The path sampler extracts reference signals for heading and velocity of the vehicle and the lateral error to the path. Then, a steering- and a velocity controller adjust the steering control variable u_δ and the acceleration input u_a, respectively, so that the vehicle follows the path and the given velocity profile. To compensate deviations from the intended path, the position and orientation is measured by a GPS-based localization system (POS LV, Applanix Inc., Richmond Hill, Ontario, Canada) and feed back to the control system. Further, the velocity v is measured. The control system is implemented in C++ using the ROS-framework [1] .

3. VEHICLE MODEL AND TRAJECTORY

To describe the motion dynamics of the vehicle, the kinematic bicycle model [Paden et al. (2016)] (Fig. 2) is considered.

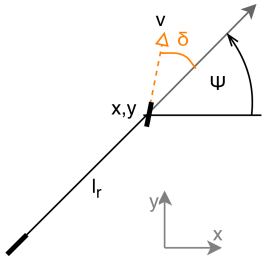

Fig. 2. Kinematic bicycle model to approximate the 4-wheeled car. The middle of the front axis is (x,y).

The model equations are given by

$$\dot{\boldsymbol{z}} = f(v, \Psi, \delta) = \begin{pmatrix} \dot{x} \\ \dot{y} \\ \dot{\Psi} \end{pmatrix} = \begin{pmatrix} v\cos(\Psi+\delta) \\ v\sin(\Psi+\delta) \\ v/l_r \cdot \sin(\delta) \end{pmatrix}. \tag{1}$$

The vector $\boldsymbol{x} := [x, y]^T$ describes the position of the middle of the front wheel axis and l_r the wheelbase. Further, Ψ is the angle between the x-axis of the global coordinate system and the vehicle body describing the orientation. Finally, δ is the steering angle. The velocity v of the front axis is given by $\dot{v} = u_a$, whereby u_a is the acceleration input.

3.1 Steering actuation

Steering is realized by a motor and an underlying controller according to the steering command u_δ. A model describing a dead-time T_δ, the steering dynamics S_δ, and a static non-linearity f_δ to describe non-linear steering [2] is used:

$$\delta(t) = f_\delta(\underbrace{S_\delta\left[u_\delta(t-T_\delta)\right]}_{\delta_m}) + \eta_\delta(t). \tag{2}$$

$$\delta = f_\delta(\alpha) = c_1\,\alpha + c_2\alpha^2\,\mathrm{sign}(\alpha)$$

The input is the control variable u_δ and t denotes the time. Uncertainties (e.g., in f_δ) are introduced by the disturbance η_δ. The dynamics S_δ is approximated by the transfer function $G_\delta(s) = \omega_\delta/(s+\omega_\delta)$, wherein s is the Laplacian variable. Its output δ_m can be measured.

3.2 Trajectory definition

The reference path (c.f. Fig. 3) is given by the functions $x_p(d)$ and $y_p(d)$, wherein d is the distance along the path.

[1] Robotic Operating System https://www.ros.org
[2] Please note: only parameters c_1, c_2 that yield a monotonically increasing function $\delta(\delta')$ are considered.

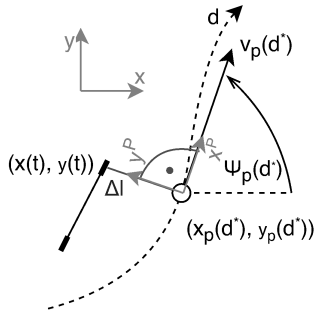

Fig. 3. The reference path (dashed line) described in the global coordinate frame by $(x_p(d)\ ,\ y_p(d))$.

In addition, a velocity profile $v_p(d)$ along the path is given. The distance $d = d(t)$ is a function of the time t.[3] Further, the path orientation angle is defined as the angle between the x-axis of the global frame and the tangent of the path:

$$\Psi_p(d) := \arg\left[\frac{\partial}{\partial d}x_p(d), \frac{\partial}{\partial d}y_p(d)\right]^T. \tag{3}$$

The vehicle displacement to the path is described by

$$\Delta\boldsymbol{x} := \boldsymbol{x} - \boldsymbol{x}_p(d). \tag{4}$$

By transforming $\Delta\boldsymbol{x}$ into the path-frame P, the quantities Δd and Δl for the longitudinal and lateral displacement, respectively, are defined by $[\Delta d, \Delta l]^T = \Delta\boldsymbol{x}^P$ [4], whereby

$$\Delta\boldsymbol{x}^P := \boldsymbol{R}^{-1}(\Psi_p(d))\Delta\boldsymbol{x}, \quad \boldsymbol{R}(a) := \begin{pmatrix}\cos a & -\sin a\\ \sin a & \cos a\end{pmatrix}. \tag{5}$$

Herein $\boldsymbol{R}$ is the standard rotation matrix.

4. INVERSION BASED CONTROL

The aim is to find a controller for the steering angle control variable u_δ that causes the vehicle to follow the given path independent on the vehicle velocity v.

The two-degree of freedom steering-controller prototype

$$u_\delta(t) = S_\delta^{-1}\left[f_\delta^{-1}\left(u^*(t+T_\delta) + \Delta u(t)\right)\right] \tag{6}$$

is proposed to invert the model (2) introducing the augmented control variables u^* and Δu. Herein, u^* is used to perform path tracking in absence of disturbances $\eta_\delta = 0$ in a feedforward fashion. Disturbances are then compensated by a feedback component Δu.

Herein, the inverse dynamics S_δ^{-1} is approximated by the transfer function $G^\dagger(s) = \omega^\dagger/\omega_\delta \cdot (s+\omega_\delta)/(s+\omega^\dagger)$, $\omega^\dagger \gg \omega_\delta$. In the ongoing argumentation $G^\dagger \cdot G_\delta \approx 1$ is assumed. The delay T_δ in Eq. (2) is cancelled by a time-shift of u^* by T_δ.

The result of applying the controller prototype (6) to (2) is

$$\delta(t) = \eta_\delta(t) + u^*(t) + \Delta u(t - T_\delta). \tag{7}$$

[3] Properties: $d(0) = 0$, $d(t) \geq 0$ for $t \geq 0$, d is strictly monotonically increasing as the vehicle can only move forward ($v > 0$).

[4] Δd and Δl describe the displacement of the vehicle position compared to where it should be (ideally small). The base coordinate system P for these two quantities is aligned to the path. The base vector corresponding to Δd points into the direction of the path.

Notation The hypothetical case in which the vehicle exactly follows the path (in absence of disturbances and model uncertainties) is called *nominal case* and the belonging symbols will be denoted by the superscript "*". Variables describing deviations to exact path tracking as given by, e.g., Δu are denoted by "Δ". All quantities $(.)_r$ denoted by the index r are reference signals.

4.1 Path tracking

The aim is to steer the vehicle so that it follows the path $x_p(d) = x(t)$, $y_p(d) = y(t)$, $\forall t > 0$. These conditions are equivalent to

$$\dot{\boldsymbol{x}} = \begin{pmatrix}\dot{x}(t)\\ \dot{y}(t)\end{pmatrix} = \frac{\partial}{\partial t}\begin{pmatrix}x_p(d(t))\\ y_p(d(t))\end{pmatrix} = \frac{\partial}{\partial t}d(t) \cdot \frac{\partial}{\partial d}\begin{pmatrix}x_p(d)\\ y_p(d)\end{pmatrix} \tag{8}$$

$$\boldsymbol{x}(0) = \begin{pmatrix}x(0)\\ y(0)\end{pmatrix} = \begin{pmatrix}x_p(d(0))\\ y_p(d(0))\end{pmatrix}. \tag{9}$$

By taking the argument and the absolute value of $\dot{\boldsymbol{x}}$, using Eq. (3), and applying the model (1)

$$\arg\dot{\boldsymbol{x}} = \Psi(t) + \delta(t) = \Psi_p(d(t)) \tag{10}$$

$$|\dot{\boldsymbol{x}}| = v = \frac{\partial}{\partial t}d(t) \tag{11}$$

are obtained. Using Eq. (10), the steering angle causing the vehicle to track the path is then given by

$$\delta(t) = \Psi_p(d(t)) - \Psi(t). \tag{12}$$

To fulfill velocity condition (11), two options are available:

(1) Using a fixed function d (i.e., a fixed velocity profile) and control the velocity v to track the profile v_p.
(2) Adapting $d(t)$ during active control so that it matches to the vehicle velocity $v(t)$ and fulfills Eq. (11).

Please note that in the first option, the path tracking performance depends on the velocity-tracking performance. In the second option, however, path tracking is independent and, hence, decoupled from the velocity. Therefore, the latter is chosen.

4.2 Path sampling

During active control, d is continuously determined depending on the position (x, y) so that the x-component of the displacement vector in the path frame $\Delta\boldsymbol{x}^P$ is zero ($\Delta d = 0$), yielding d^*:

$$[\Delta d, \Delta l]^T = \Delta\boldsymbol{x}^P(d = d^*), \quad \Delta d = 0. \tag{13}$$

Please note that $\Delta d = 0$ causes the displacement vector to be perpendicular to the path tangent in d^*. Further, this yields the shortest Euclidean distance between the path $(x_p(d^*(t)), y_p(d^*(t)))$ and the current vehicle position $(x(t), y(t))$.[5] Hereby, the lateral distance to the path Δl is introduced.

Finally, the velocity projected onto the path is defined by:

[5] It is assumed that the lateral distance to the path Δl does not exceed the curve radius.

$$v^*(t) := \frac{\partial}{\partial t} d^*(t). \tag{14}$$

Then, the reference signals for the controller are the sampled path orientation angle $\Psi_r(t) := \Psi_p(d^*(t))$ and the sampled velocity profile $v_r(t) := v_p(d^*(t))$. The dynamics of the displacement $\Delta\boldsymbol{x}$ for $d = d^*$ is analyzed in Sec. 5.1.

4.3 Controller

Using result (12), the time-shifted path tracking u^* is

$$u^*(t + T_\delta) = \Psi_r(t + T_\delta) - \Psi(t + T_\delta). \tag{15}$$

The future vehicle orientation $\Psi(t + T_\delta)$ is approximated by $\Psi(t + T_\delta) \approx \Psi(t)$.[6] Further, the ahead-of-time path sampling is approximated by the prediction $\Psi_r(t + T_\delta) \approx \Psi_p(d^*(t) + v(t)\, T_\delta)$. Herein, a constant velocity $v(t)$ within the prediction horizon $[t, t + T_\delta]$ is assumed yielding

$$u^*(t + T_\delta) \approx \Psi_p(d^*(t) + v(t)\, T_\delta) - \Psi(t). \tag{16}$$

5. PATH DEVIATION DYNAMICS

In this section, the effect of the linearizing controller (6) is investigated. Herein, deviations (in terms of the lateral error and the orientation misalignment) to the intended driving path are considered. Therefore, a dynamic model describing the closed-loop dynamics of the path tracking controller applied to the vehicle model (Δ-dynamics) is derived. Herein, n exact inversion of the steering model is assumed as described by Eq. (7). This closed-loop system depends on the virtual steering angle Δu. Quantities for the lateral- and orientation deviation are introduced, and their relationship to the virtual control input Δu is investigated. This, in turn, allows to design compensators for deviations from the path.

To simplify the notation, $\eta_\delta = 0$ is assumed. Without loss of generality, a steering disturbance can still be treated as an additive disturbance to Δu. The system is given by

$$\begin{pmatrix} \dot{\Delta\boldsymbol{x}} \\ \dot{\Delta\Psi} \end{pmatrix} = f(v, \Psi, \delta)\,|_{\delta=\delta^*+\Delta u(t-T_\delta)} - f(v, \Psi, \delta)\,|_{\delta=\delta^*}. \tag{17}$$

Fig. 4 shows an overview of variables introduced in this section and their geometric interpretation. To further shorten the notation $\Delta u^d(t) := \Delta u(t - T_\delta)$ is introduced.

5.1 Lateral error

Regarding the displacement $\Delta\boldsymbol{x}$, Eq. 17 yields

$$\dot{\Delta\boldsymbol{x}} = v\boldsymbol{R}(\Psi_r)\begin{pmatrix}\cos(\Delta u^d)\\ \sin(\Delta u^d)\end{pmatrix} - v^*\boldsymbol{R}(\Psi_r)\begin{pmatrix}1\\0\end{pmatrix}. \tag{18}$$

The displacement dynamics shall now transformed into the path frame P. By taking the derivative of Eq. (5), substituting $\boldsymbol{\Delta x} = \boldsymbol{R}(\Psi(d(t)))\boldsymbol{\Delta x}^P$ (c.f. Eq. (5)), $d = d^*$, and using Eq. (13) ($\boldsymbol{\Delta x}^P = [0, \Delta l]^T$)

[6] As shown in Sec. 5.2, Ψ results from Ψ_r as described by a low-pass dynamics (c.f. Eq. (20)). Hence, the rate of change of Ψ typically low, in comparison. Therefore, $\Psi(t) \approx \Psi(t + T_\delta)$ is assumed.

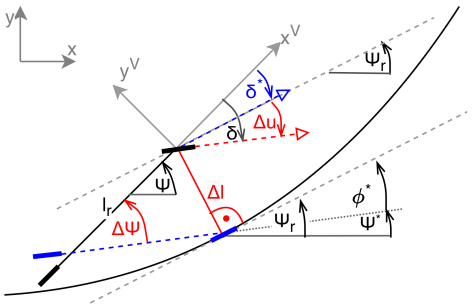

Fig. 4. The vehicle geometry and the Δ-variables introduced the by tracking controller. Shown are the angles in case the vehicle is exactly following the path (dashed vehicle, colored in blue) and the Δ-angles describing the vehicle relative to the path (in red).

$$\frac{\partial}{\partial t}\boldsymbol{\Delta x}^{\boldsymbol{P}} = \begin{pmatrix}\dot{\Delta d}\\ \dot{\Delta l}\end{pmatrix} = \begin{pmatrix}\Delta l\, \dot{\Psi}_r(t)\\ 0\end{pmatrix} + \begin{pmatrix} v\cos(\Delta u^d) - v^*\\ v\sin(\Delta u^d)\end{pmatrix}.$$

is obtained. Please recap, that Δl is the lateral distance of the vehicle to the path (Fig. 4). Further, please note that $\Delta d = 0 \Rightarrow \dot{\Delta d} = 0$ holds (c.f. Eq. (13)) yielding a relationship between v and v^*. In conclusion, by choosing $d = d^*$ (c.f. Sec. 4.2), the lateral dynamics is given by

$$\dot{\Delta l} = v\sin(\Delta u^d), \quad \dot{\Delta l}(0) = \Delta l_0, \tag{19}$$

wherein Δl_0 is the initial lateral error.

5.2 Vehicle orientation

Similar to the deviation in the position, the deviation to the nominal orientation $\Delta\Psi$ is investigated as defined by Eq. (17). First, the nominal case ($\Delta u = 0$, the right hand side of Eq. (17)) is considered. Therefore, the nominal vehicle orientation Ψ^* is introduced by applying $\delta = \delta^*$:

$$\dot{\Psi}^* := \dot{\Psi}|_{\delta=\delta^*} = \frac{v}{l_r}\sin(\Psi_r - \Psi^*). \tag{20}$$

This equation serves as an internal model in the controller. The initial value $\Psi^*(0)$ is set to the measured vehicle orientation at controller initialization:

$$\Psi^*(0) := \Psi(0). \tag{21}$$

To simplify the notation, the orientation gap $\phi^* := \Psi_r - \Psi^*$ to the path is introduced. Then, the dynamics of $\Delta\Psi = \Psi - \Psi^*$ (the difference between the orientation to the nominal vehicle orientation) is calculated from Eq. (17) yielding

$$\dot{\Delta\Psi} := \frac{v}{l_r}\left[\sin(\Psi_r - \Psi + \Delta u^d) - \sin(\Psi_r - \Psi^*)\right].$$

Finally, replacing $\Psi = \Delta\Psi + \Psi^*$ yields

$$\dot{\Delta\Psi} = \frac{v}{l_r}\left[\sin(\phi^* - \Delta\Psi + \Delta u^d) - \sin(\phi^*)\right]. \tag{22}$$

6. PATH TRACKING STABILIZATION

Based on the Δ-dynamics derived in Sec. 5, a state-feedback controller is used to keep the vehicle on the path. Herein, an orientation-feedback stabilizes vehicle (e.g., in

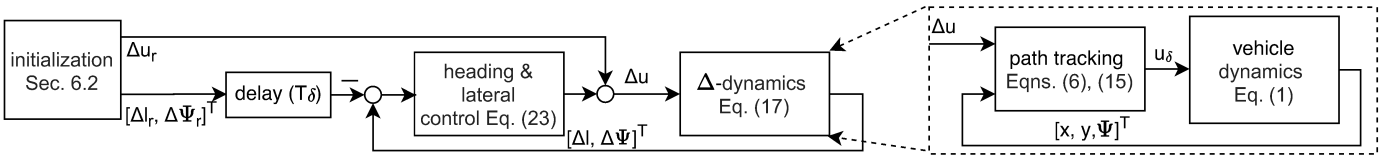

Fig. 5. Overview of the steering control system. The Δ-dynamics results from the closed-loop path tracking controller.

case of slipping). An overview of the control scheme is given in Fig. 5. The state in which the vehicle exactly follows the path ($\Delta l = \Delta\Psi = 0$) is called steady-state. To compensate steady-state errors, the controller-internal integrator states x^I and x^{II} are introduced and, further, used for state feedback. To partially cancel the dependency on the velocity, the control variable is modulated by the inverse velocity $1/v$. The controller equations are given by

$$\Delta u = \frac{l_r}{v} \underbrace{\left[-k_\Psi\, e_{\Delta\Psi} - k_p\, e_{\Delta l} - k_i x^I - k_{ii} x^{II}\right]}_{:=U(t)} + \Delta u_r$$
$$\dot{x}^I = e_{\Delta l},\ \dot{x}^I(0) = 0,\ \dot{x}^{II} = x^I,\ x^{II}(0) = 0,\ v > 0. \quad (23)$$

Herein, the state-feedback gains are $k_\Psi \geq 0$, $k_p \geq 0$, $k_i \geq 0\, k_{ii} \geq 0$. Further, the feedback variables $e_{\Delta l} = (\Delta l - \Delta l_r)$ and $e_{\Delta\Psi} = (\Delta\Psi - \Delta\Psi_r)$ are introduced wherein Δl_r and $\Delta\Psi_r$ are reference signals. The control loop might be initialized in presence of non-zero initial states (i.e., in case the vehicle is initially not aligned to the path). In this case, the references Δl_r, $\Delta\Psi_r$, and Δu_r allow to realize a defined convergence to the steady-state (c.f. Sec. 6.2).

6.1 Stability

To perform a stability analysis, the non-linear Δ-dynamics is linearized. Then, the eigenvalues are investigated.

By applying the controller (Eq. (23)) to the orientation model (Eq. (22)) the closed-loop dynamics for the orientation is obtained:

$$\dot{\Delta\Psi} = \frac{v}{l_r}\left[\sin(\phi^* - \Delta\Psi + \frac{l_r}{v}U(t - T_\delta)) - \sin(\phi^*)\right].$$

By assuming small angles, a linear approximation is [7]

$$\dot{\Delta\Psi} = -\frac{v}{l_r}\Delta\Psi + U(t - T_\delta). \quad (24)$$

Similar, by applying the controller Eq. (23) to the lateral dynamics Eq. (19)

$$\dot{\Delta l} = v \sin\left(\frac{l_r}{v}U(t - T_\delta))\right)$$

is obtained, which approximated by

$$\dot{\Delta l} = l_r U(t - T_\delta). \quad (25)$$

Combining Eqns. (25), (24), and (23) and assuming ($T_\delta = 0$) yields the state-space system

$$\begin{pmatrix} \dot{\Delta\Psi} \\ \dot{\Delta l} \\ \dot{x}^I \\ \dot{x}^{II} \end{pmatrix} = \underbrace{\begin{pmatrix} -\frac{v}{l_r} - k_\Psi & -k_p & -k_i & -k_{ii} \\ -k_\Psi l_r & -k_p l_r & -k_i l_r & -k_{ii} l_r \\ 0. & 1 & 0 & 0 \\ 0. & 0 & 1 & 0 \end{pmatrix}}_{:=\boldsymbol{A}} \cdot \begin{pmatrix} \Delta\Psi \\ \Delta l \\ x^I \\ x^{II} \end{pmatrix}.$$

Please note that the dependency on the velocity is canceled by the controller, except for the orientation ($\Delta\Psi$) dynamics. The linearized closed loop is asymptotically stable for a constant velocity v, iff all eigenvalues of $\boldsymbol{A}$ are asymptotically stable. To prevent singularities, the controller is only active for a minimum velocity $v > v_{min}$. [8]

6.2 Controller initialization

Please note, that on controller activation ($t = 0$), the vehicle is not necessarily aligned to the path, i.e., orientation and lateral displacement are present. In addition, the steering angle δ has an initial state $\delta(0)$ not necessarily fulfilling the path tracking constraint Eq. (12). This is equivalent to a non-zero initial Δ-steering angle $\Delta u(0)$. Without measures ($\Delta l_r = \Delta\Psi_r = \Delta u_r = 0$), the feedback controller does not necessarily perform a transition to steady-state by applying acceptable amplitudes in the steering angle and steering rate. E.g., limits for the lateral acceleration might be exceeded. Therefore, as shown in Fig. 7, a defined, transient approaching to the steady-state is realized by applying transients to Δl_r, $\Delta\Psi_r$ and Δu_r (c.f. Sec. (6)) that lead to a defined convergence to the intended path, while satisfying given motion constraints.

The initial conditions for $\Delta\Psi$ [9], Δl [10], and Δu [11] are

$$\Delta\Psi_0 := \Delta\Psi(0) = \Psi(0) - \Psi^*(0) = 0, \quad (26)$$
$$\Delta l_0 := \Delta l(0), \quad (27)$$
$$\Delta u_0 := \Delta u(0) = f_\delta(\delta_m(0)) - u^*_\delta(0), \quad (28)$$
$$u^*_\delta(0) = \Psi_r(0 + T_\delta) - \Psi(0). \quad (29)$$

Initialization transients A controller-internal virtual control-loop is used to define the approach to steady-state

[7] The simplification is valid for $\phi^* \approx 0$ and $\Delta u \approx 0$. Larger values of ϕ^* can appear in curves with a short curve radius (c.f. Fig. 4).

[8] Driving slower than v_{min} is supported only for a short duration not causing the vehicle to significantly drift off the path, e.g., when doing a full-stop or moving off. In case the controller is deactivated, the latest steering angle is hold until the controller is reactivated.

[9] The initial Δ-orientation $\Delta\Psi$ is obtained using (Eq. (21) and $\Delta\Psi = \Psi - \Psi^*$).

[10] The initial lateral error Δl is measured as described in Sec. 4.2.

[11] The initial Δ-steering angle Δu_0 is obtained by calculating the initial path tracking controller output $u^*(0)$ (Eq. (15)), the tracking controller (Eq. (6)), and the steering angle measurement by constraining $u_\delta(0) = \delta_m(0)$ (Eq. (2)). The absence of steering disturbances $\eta_\delta = 0$ and a steady-state of the steering dynamics S_δ are assumed.

[12] The vehicle acceleration vector $[\ddot{x}, \ddot{y}]^T$ projected onto the y-axis of the vehicle frame V (c.f. Fig. 4).

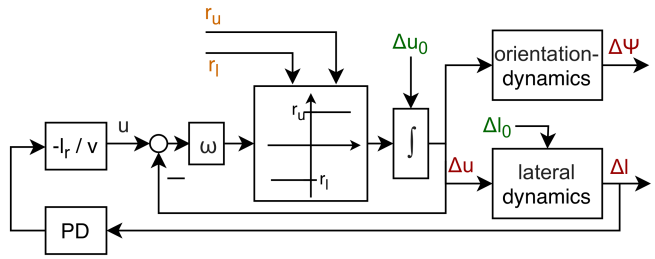

Fig. 6. Controller internal virtual control-loop simulating a defined approach to steady-state. Herein, the steering rate is limited ($r_l < \dot{\Delta u} < r_u$) as realized by saturating the input to the integrator block that yields Δu. The computed signals Δl, $\Delta\Psi$, and Δu then serve as references Δl_r, $\Delta\Psi_r$, and Δu_r to the controller.

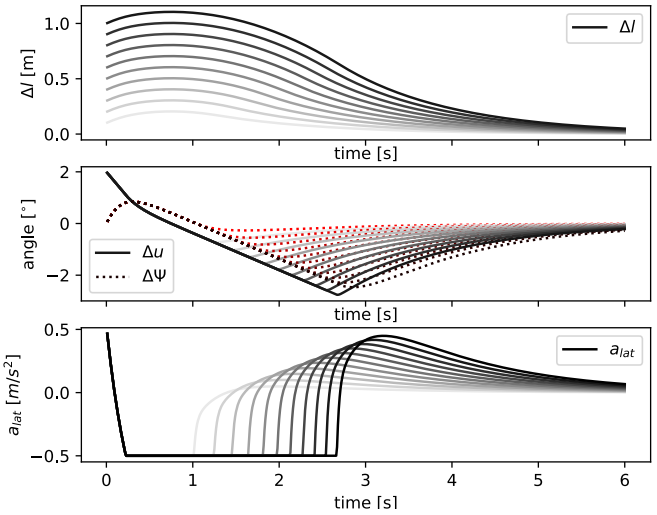

Fig. 7. Exemplary approaching to steady-state for a set of non-zero initial lateral errors $0 \leq \Delta l_0 \leq 1\,\mathrm{m}$ and an initial steering angle $\Delta u_0 = 2°$ while driving with a constant velocity $v = 10\,\mathrm{m/s}$ on a straight path ($\phi^* = 0$). As the steering-rate is limited, the lateral error increases for a short time-period until it converges to zero. Shown are the delta-steering angle Δu and delta-orientation $\Delta\Psi$. Further, the lateral acceleration $a_{lat} = v(\dot{\Delta\Psi} + \dot{\Delta u})\cos(\Delta u)$ [12] is shown.

(c.f. Fig. 6). Therefore, an internal model of the Δ-dynamics and a virtual PD-controller $u = \frac{l_r}{v}(-k_1\,\Delta l - k_2\,\dot{\Delta l})$ to compensate the initial lateral error $\Delta_l(0)$ are used.

The absolute vehicle acceleration is given by

$$a_{abs} = |[\ddot{x}, \ddot{y}]^T| = |\dot{v}| + |v||\dot{\Psi} + \dot{\delta}| \quad (30)$$

$$= |\dot{v}| + |v||\dot{\Psi}^* + \dot{\Delta\Psi} + \dot{\delta}^* + \dot{\Delta u}| \quad (31)$$

To simplify the argumentation, only the acceleration caused by the path-approaching is considered, i.e., the case of approaching to a straight path ($\phi^* = 0$, $\dot{\delta}^* = 0$, $\dot{\Psi}^* = 0$):

$$\Delta a_{abs} = |\dot{v}| + |v||\dot{\Delta\Psi} + \dot{\Delta u}|. \quad (32)$$

To limit $\Delta a_{abs} < a_{max}$, the steering rate $\dot{\Delta u}$ is limited to the range $[r_l, r_u]$, whereby r_l and r_u are continuously computed by

$$r_l(t) = -\frac{a_{max}}{v} - \dot{\Delta\Psi} \quad r_u(t) = +\frac{a_{max}}{v} - \dot{\Delta\Psi}. \quad (33)$$

The rate-limiter is realized as shown in Fig. 6. To ensure passenger comfort, the acceleration limited is set to $a_{max} = 0.5\mathrm{m/s}^2$. Further, in addition to Eq. (33), to effectively limit the steering rate also in case of low velocities, r_l and r_u are saturated to remain within $\pm 4°/\mathrm{s}$.

In case $\dot{\Delta u}$ is not saturated, the filter given by the transfer function $G = \omega/(s+\omega)$ models the steering dynamics. Herein, s is the Laplacian variable and $\omega = 20\,1/\mathrm{s}$ the cut-off frequency that is conservatively chosen so that the step-response of G is slower than the response of the real vehicle hardware S_δ.

To determine the parameters k_1 and k_2, a limited set of initial states $\Delta l_0 \in [-1\mathrm{m}, +1\mathrm{m}]$ and $\Delta u_0 \in [-3°, +3°]$ is considered. In case these bounds are exceeded, the controller cannot be activated. In the hypothetic case of absent steering rate limits, the parameters PD-parameters $k_1 = 0.4$ and $k_2 = 0.2$ yield an approaching to the path within $3\,s$ without overshoot.

Please note, that the rate limit might harm the stability of the closed-loop (e.g., [Klyde and Mitchell (2004)]). Therefore, a simulation analysis (excerpts shown in Fig. 7) with velocities ranging from 0 to 15 m/s is performed indicating the stability of the non-linear closed-loop in within the considered limits for the initial states Δl_0 and $\Delta\Psi_0$.

On controller activation, the virtual control-loop is initialized by setting the initial states as given by Eqns. (26), (27), and (29). Then, the transients Δl_r, $\Delta\Psi_r$ and Δu_r are calculated depending on the velocity v of the real vehicle and applied to the state-feedback controller (Eq. (23)) as illustrated in Fig. 5. A delay by T_δ adapts the references to the dead-time of the steering dynamics.

7. VELOCITY CONTROL

The velocity is manipulated by the acceleration input u_a. To design the controller, the internals of the combustion engine and underlying controllers implemented in the vehicle are neglected and the relationship

$$\dot{v}(t) = u_a(t - T_v) \quad (34)$$

is assumed. Herein, T_v describes the delay of the system. To track the ahead-sampled velocity reference $v_r(t+T_v) \approx v_p(d^* + vT_v)$, a 2-DoF velocity controller as shown in Fig. 8 is used. On initialization, the measured velocity $v(0)$ might differ to the reference $v_r(0)$. Hence the reference signal r_v is modified so that the new reference r'_v matches the vehicle velocity on activation: $r'_v(0) = v(0)$. This causes a non-zero error $e_r := r'_v - r_v$. As time progresses, $r'_v(t)$ is determined so that $e_r(t)$ converges to zero with a fixed rate of $|\dot{e}_r| = 1m/s^2$. Hence, a transient approach to the

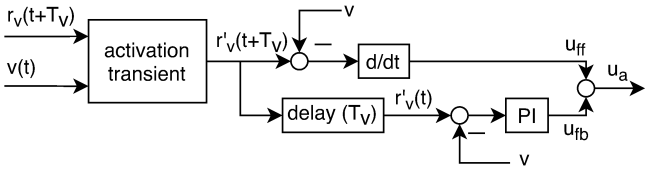

Fig. 8. The used velocity controller combining a feedforward (ff) and feedback path (fb).

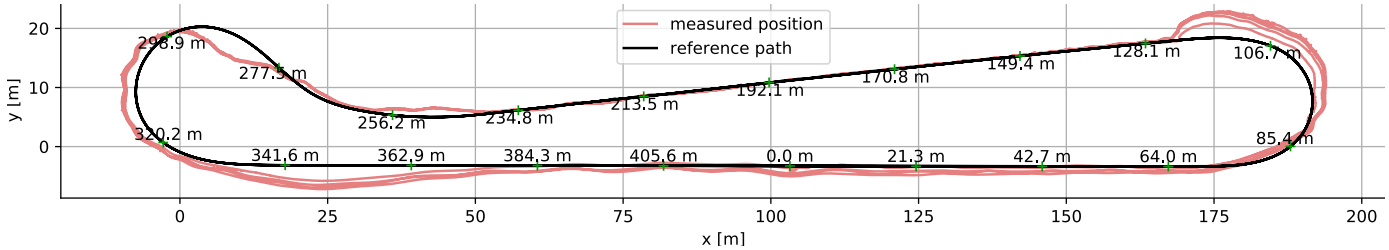

Fig. 9. The path used to test the controller and the traces of the vehicle of four turns. For a better visualization, the lateral error to the path is amplified by factor 20. The distance markings relate to the distance shown in Fig. 11.

target velocity with limited acceleration is realized. The derivative in the feedforward path causes the output v to follow changes in the reference yielding $r'_v(t) = v(t)$ in the nominal case. Disturbances are then compensated by the PI-controller.

8. PARAMETER TUNING

Identification of the steering function To determine the delay T_δ and ω_δ, the step-response of the relation between u_δ and δ_m is determined yielding $T_d = 0.03\,\mathrm{s}$ and $\omega_\delta = 28\,1/\mathrm{s}$. Then, $\omega^\dagger = 100\,1/\mathrm{s}$ is chosen to approximately invert the dynamics S_δ. To identify the parameters c_1 and c_2 of the steering function f_δ, and the wheelbase l_r, a manual driving experiment is performed. Herein, different curve radii and velocities within the intended operational scope of the controller are considered. I/O-data for the measured steering angle δ_m (c.f. Eq. (2)) and the vehicle orientation Ψ are recorded. Then, the Prediction Error Method (PEM) is used to minimize the prediction error for the output Ψ yielding $c_1 = 0.8884$, $c_2 = 0.1933$, and $l_r = 3\,\mathrm{m}$.

Steering control In a first step, the parameter k_Ψ of the orientation feedback loop is determined for the deactivated lateral compensation ($k_p = k_i = k_{ii} = 0$). The linear state-space system without delay ($T_\delta = 0$) is considered (c.f. Sec. 6.1). To obtain a rise time of $0.5\,s$ in $\Delta\Psi$ in the response to a step-wise disturbance, $k_\Psi = 1.6$ is chosen. The localization, unconsidered dynamics in the vehicle mechanics, and the implementation on a non-realtime system introduce further uncertain delays in the closed loop. Hence, the proportional gain k_p is experimentally determined. For deactivated integral control ($k_i = 0$ and $k_{ii} = 0$), $k_p = 0.62$ minimizes the time needed to compensate a lateral error without noticeable overshoot. The integral gain $k_i = 0.45$ causes linearly increasing disturbances to Δl (e.g., due to side wind) to be compensated within $\approx 4\,\mathrm{s}$. In experimental tests, a remaining steady-state error in Δl when leaving curves and continuously accelerating was observed. Therefore, the double integral controller is activated by choosing $k_{ii} = 0.12$. To verify the stability, the eigenvalues of the resulting closed-loop system (c.f. Sec. 6.1) are visualized in Fig. 10 for $v \in [0, 30\,\mathrm{m/s}]$.

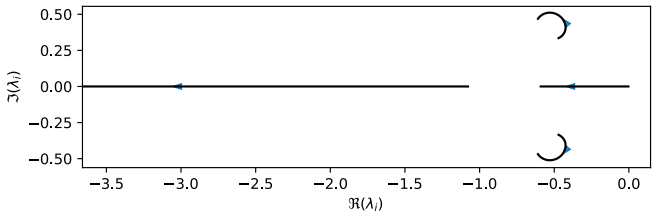

Fig. 10. Eigenvalues of the closed-loop steering dynamics (c.f. Sec. 6.1) for a varying velocity $0 < v < 30\,\mathrm{m/s}$.

Finally, the minimal velocity to activate the steering controller $v_{min} = 0.3\,\mathrm{m/s}$ is chosen to not hinder typical driving scenarios while not causing significant lateral deviations during vehicle stop and start.

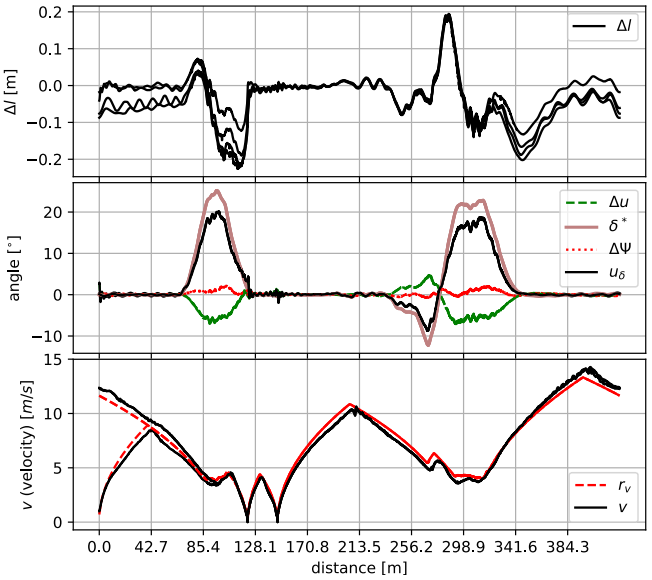

Fig. 11. The results for four driving cycles: the presented data is segmented for each turn and aligned to the distance markers shown in Fig. 9.

Velocity control The delay of $T_{d,v} = 0.02\,\mathrm{s}$ matches the typical delay observed in I/O data. As the detailed model of the combustion engine is uncertainly known, the parameters $k_{p,v} = 0.6$ and $k_{i,v} = 0.05$ of the PI-controller (Sec. 7) were experimentally chosen to cause a step response of 1 s while allowing 10 % overshoot.

9. RESULTS

The control system performance was evaluated in a driving-control test involving the Volvo XC-90 car on a closed test-ground. Therefore, the map as shown in Fig. 9 is used by the trajectory planner to generate reference trajectories. Herein, the velocity profile is adapted to the curvature (10m to ∞) of the path to not exceed a lateral acceleration of $1\,\mathrm{m/s^2}$. Although a mode for an electric-only drive train is available, the use of the combustion engine was intentionally enforced to challenge the decoupling of the velocity in path tracking.

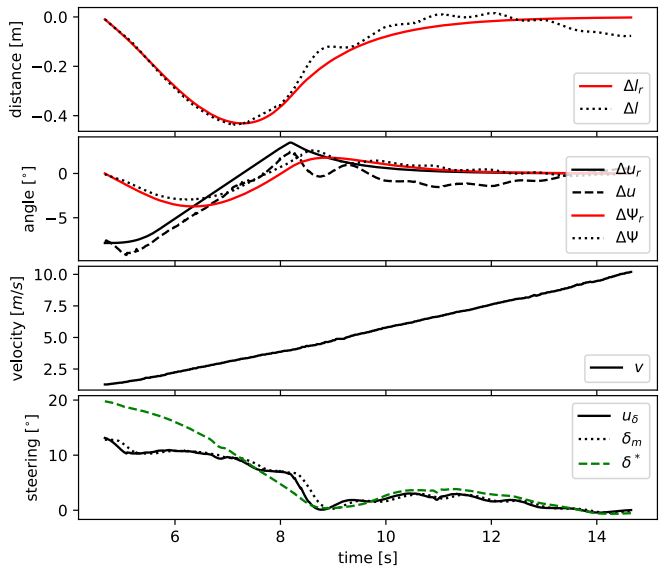

Fig. 12. Exemplary results for controller initialization.

The results for four automatic driving cycles are given in Figs. 9 and 11. As expected, the lateral error increases in curves, however, not exceeding 22.6 *cm*. The orientation difference $\Delta\Psi$ remains below 4° indicating a stable vehicle orientation. The RMSE is calculated along the distance variable for the lateral error is 7.2 cm.

An exemplary handover inside a curve from a human driver is given in Fig. 12. Due to the unaligned vehicle orientation and steering, the lateral displacement is intentionally increasesed up to 40 cm to reduce the steering activity.

10. CONCLUSION

A path tracking controller for autonomous driving is proposed. In a test on a closed ground, the lateral RMS-error was 7.2 cm which is significantly smaller than the typical inter-vehicle distance observed in urban driving scenarios. Further, in curves, a maximal error of 22.6 cm was observed.

For the given application, the control design using a simpler kinematic model requiring fewer parameters seems feasible. The decoupling of the velocity further relaxed the requirements on a longitudinal model: the manual tuning of a linear 2 DoF velocity controller is feasible to control the combustion engine without disturbing path tracking. Then, to adapt the steering controller to the vehicle, a manual driving test to determine the nonlinear steering parameters and the manual tuning of the proportional gain, are sufficient to obtain the needed parameters to control steering. In comparison to MPC, the computational requirements are low and the algorithm is time-deterministic.

It is important to note that, the rate of change of the steering control variable (and therefore the lateral acceleration) is sensitive to the reference trajectory. Therefore, the path and the velocity profile need to be chosen to not introduce jerk in the vehicle motion. Though the control system positions the front-wheel, tracking of any point of the vehicle can be realized by appropriately transforming the reference path.

Some controller gains were experimentally chosen as uncertain delays are present yielding lower values than theoretically possible. Hence, for the absence of delays, improved tracking performance is expected. Additionally, a steering disturbance observer might be used to further enhance performance.

In future investigations, the robustness to lateral slipping and over- and understeering will be investigated in simulation and on the proving-ground.

REFERENCES

Attia, R., Orjuela, R., and Basset, M. (2014). Combined longitudinal and lateral control for automated vehicle guidance. *Vehicle System Dynamics*, 52(2), 261–279. doi:10.1080/00423114.2013.874563. URL `https://doi.org/10.1080/00423114.2013.874563`.

Falcone, P., Borrelli, F., Asgari, J., Tseng, H.E., and Hrovat, D. (2007). Predictive active steering control for autonomous vehicle systems. *IEEE Transactions on Control Systems Technology*, 15(3), 566–580. doi: 10.1109/TCST.2007.894653.

Guo, J., Hu, P., and Wang, R. (2016). Nonlinear coordinated steering and braking control of vision-based autonomous vehicles in emergency obstacle avoidance. *IEEE Transactions on Intelligent Transportation Systems*, 17(11), 3230–3240.

Khodayari, A., Ghaffari, A., Ameli, S., and Flahatgar, J. (2010). A historical review on lateral and longitudinal control of autonomous vehicle motions. In *2010 International Conference on Mechanical and Electrical Technology*, 421–429. IEEE.

Klyde, D.H. and Mitchell, D.G. (2004). Investigating the role of rate limiting in pilot-induced oscillations. *Journal of guidance, control, and dynamics*, 27(5), 804–813.

Marino, R., Scalzi, S., and Netto, M. (2011). Nested pid steering control for lane keeping in autonomous vehicles. *Control Engineering Practice*, 19(12), 1459 – 1467. doi: https://doi.org/10.1016/j.conengprac.2011.08.005.

Menhour, L., d'Andréa Novel, B., Fliess, M., and Mounier, H. (2014). Coupled nonlinear vehicle control: Flatness-based setting with algebraic estimation techniques. *Control Engineering Practice*, 22, 135–146.

Paden, B., Čáp, M., Yong, S.Z., Yershov, D., and Frazzoli, E. (2016). A survey of motion planning and control techniques for self-driving urban vehicles. *IEEE Transactions on Intelligent Vehicles*, 1(1), 33–55. doi: 10.1109/TIV.2016.2578706.

Shivam, S., Buckley, I., Wardi, Y., Seatzu, C., and Egerstedt, M. (2019). Tracking control by the newton-raphson flow: Applications to autonomous vehicles. In *2019 18th European Control Conference (ECC)*, 1562–1567. IEEE.

Thrun, S., Montemerlo, M., Dahlkamp, H., Stavens, D., Aron, A., Diebel, J., Fong, P., Gale, J., Halpenny, M., Hoffmann, G., et al. (2006). Stanley: The robot that won the darpa grand challenge. *Journal of field Robotics*, 23(9), 661–692.

Xia, Y., Pu, F., Li, S., and Gao, Y. (2016). Lateral path tracking control of autonomous land vehicle based on adrc and differential flatness. *IEEE Transactions on Industrial Electronics*, 63(5), 3091–3099.